Published OnlineFirst March 11, 2020; DOI: 10.1158/1078-0432.CCR-19-2238

OMTX705, a Novel FAP-Targeting ADC Demonstrates Activity in Chemotherapy and Pembrolizumab-Resistant Solid Tumor Models

Myriam Fabre[1], Cristina Ferrer[1], Saioa Domínguez-Hormaetxe[1], Bruno Bockorny[2], Laura Murias[1], Oliver Seifert[3], Stephan A. Eisler[3], Roland E. Kontermann[3], Klaus Pfizenmaier[3], So Young Lee[4], María dM. Vivanco[4], Pedro P. López-Casas[5], Sofia Perea[2,5], Muhammad Abbas[6], Wolfgang Richter[6], Laureano Simon[1], and Manuel Hidalgo[5,7]

ABSTRACT

Purpose: The tumor microenvironment plays a key role in cancer development and progression and is involved in resistance to chemo- and immunotherapy. Cancer-associated fibroblast expressing fibroblast-activating protein α (FAPα) is one of the predominant stroma cell types and is involved in resistance to immunotherapy.

Experimental Design: We generated OMTX705, a novel antibody–drug conjugate from a humanized anti-FAP antibody linked to a new cytolysin. Here, we studied its antineoplastic activity *in vitro* and in preclinical mouse models alone and in combination with chemotherapy as well as immunotherapy in PD-1–resistant tumors.

Results: In Avatar models, OMTX705 showed a 100% tumor growth inhibition and prolonged tumor regressions as single agent and in combination with chemotherapy. Treatment rechallenge following treatment discontinuation induced additional tumor regression, suggesting lack of treatment resistance. In a mouse model with a humanized immune system resistant to PD-1 inhibition, OMTX705 increased tumor infiltration by $CD8^+$ T cells, induced complete regressions, and delayed tumor recurrence.

Conclusions: These data suggest that FAP targeting with OMTX705 represents a novel and potent strategy for cancer treatment, including tumors resistant to immunotherapy, and support its clinical development.

Introduction

Solid tumors frequently exhibit a significant stromal reaction, called desmoplasia, formed by a variety of stromal cells and dense extracellular matrix. This component may represent up to 20%–60% of the total tumor mass (1). In particular, cancer-associated fibroblasts (CAF) are frequently observed within the stroma of various cancers, including breast, lung, colon, and pancreatic carcinomas (2, 3). Interacting coordinately with the different components of the stroma, CAFs have been associated with multiple cancer properties including neoangiogenesis, tumor progression, metastasis, impairment of drug delivery, and immunosuppression (3–12).

The identification of cellular and molecular targets to abrogate stroma–tumor cell interactions is one of the most active areas in anticancer drug development. In pancreatic ductal adenocarcinoma (PDAC), the number of agents targeting the stroma is rapidly increasing with several agents in phase III clinical development (13–17). In addition to tumor growth inhibition, disruption of the stroma aims at increasing intratumor drug delivery and is expected to facilitate the activity of immunotherapy agents (17–19).

The fibroblast desmoplastic response is frequently characterized by the induction of the cell surface protein fibroblast-activating protein α (FAPα). FAPα is a dimeric type II serine protease of 170 kDa which is overexpressed in more than 90% of carcinomas. FAPα has a transitory and highly restricted expression in normal adult tissues during wound healing and embryogenesis (20). No *FAP* gene expression has been reported in healthy tissues with the exception of low-level expression in adipocytes, smooth muscle, bone marrow, and uterus (21). Its highly focal expression in CAFs surrounding the tumor microvasculature, together with its fast and efficient internalization, makes this protein an attractive therapeutic target. Recently, studies have shown that FAP-expressing CAFs are a nonredundant, immunosuppressive component of the tumor microenvironment (7). Ablation of FAP-expressing cells in PDAC allowed TNFα- and IFNγ-mediated immunologic control of tumor growth (7). Moreover, depletion of FAP-expressing CAFs synergizes with anti-PD-L1 immunotherapy in PDAC suggesting that it may represent a relevant target to complement immune checkpoint inhibitors (18). Unfortunately, FAP-targeted approaches using blocking antibodies or small-molecule inhibitors have failed in phase II trials for lack of efficacy thus far (22–24).

On the basis of this rationale, we developed a novel antibody–drug conjugate (ADC) molecule to target FAP-expressing CAFs. We aimed at using the FAP protein as a docking for the ADC so that, upon FAP binding onto the CAF cell membrane, the agent is internalized and transported to intracellular late endosome where the cytotoxic moiety is released. The targeting of CAFs and the associated stroma modulation would then delay disease progression, increase drug penetration, and reestablish the tumor immune response to anti-PD-1 therapy.

[1]Oncomatryx Biopharma S.L., Derio, Spain. [2]Beth Israel Deaconess Medical Center, Harvard Medical School, Boston, Massachusetts. [3]Institute of Cell Biology and Immunology, University of Stuttgart, Stuttgart, Germany. [4]CIC BioGUNE, Derio, Spain. [5]Gastrointestinal Cancer Clinical Research Unit, Spanish National Cancer Research Centre (CNIO), Madrid, Spain. [6]TUBE Pharmaceuticals, Wien, Austria. [7]Weill Cornell Medical College, New York, New York.

Note: Supplementary data for this article are available at Clinical Cancer Research Online (http://clincancerres.aacrjournals.org/).

Corresponding Authors: Myriam Fabre, Oncomatryx Biopharma S.L., Edificio 801-B, Parque Tecnológico de Bizkaia, Derio, Bizkaia 48160, Spain. Phone: 349-4608-7037; Fax: 349-4608-7037; E-mail: mfabre@oncomatryx.com; and Manuel Hidalgo, Weill Cornell Medicine/Hematology and Medical Oncology, 1305 York Avenue, Y741, Box 403, New York, NY 10021. Phone: 646-962-2268; E-mail: mah4006@med.cornell.edu

Clin Cancer Res 2020;XX:XX–XX

doi: 10.1158/1078-0432.CCR-19-2238

Published OnlineFirst March 11, 2020; DOI: 10.1158/1078-0432.CCR-19-2238

Translational Relevance

OMTX705 is a novel, potent, antibody–drug conjugate that targets fibroblast-activating protein–positive cancer-associated fibroblasts, a critical component of the cancer stroma. The agent exerts preclinical antitumor activity as single agent, in combination with chemotherapy, and in tumors resistant to PD-1 inhibitors. These data support the clinical development of this drug for cancer treatment.

Here, we report the preclinical development of OMTX705, an ADC formed by a new humanized anti-FAP mAb (OMTX005) that has been conjugated to a novel cytolysin, TAM470, a synthetic microtubule inhibitor from the tubulysin family.

Materials and Methods

Cell lines

The fibrosarcoma cell line HT1080 wild-type (WT) and the stably transfected human or murine FAP-expressing syngeneic lines (hereafter called HT1080-FAP and HT1080-moFAP) were kindly provided by W. Rettig (Boehringer Ingelheim Pharma). Primary human CAFs (CAF07) were purchased from Neuromics. CHOK1SV GS-KO cell line was obtained from Lonza Ltd. HT1080-WT and HT1080-FAP cell lines were cultured and maintained in RPMI1640 medium supplemented with 10% FBS, 2 mmol/L L-glutamine, G418 (0.2 mg/mL) at 37°C and 5% CO_2. CHOK1SV GS-KO cells were cultured in CD-CHO media supplemented with 6 mmol/L L-glutamine. Primary human CAFs were cultured in MSC-GRO VitroPlus III, low serum complete medium (Vitro Biopharma).

In vitro viability assay

HT1080-WT and HT1080-FAP (2.5×10^3 cells/well) or CAF07 cells (1×10^4 cells/well) were seeded in a 96-well plate (100 µL medium/well) and grown overnight at 37°C. Cells were treated with serial dilutions (1:4) of antibodies OMTX705, OMTX005, or IgG Kappa-TAM558 (starting at 400 nmol/L) or serial dilutions of free drugs TAM558 and TAM470 (starting at 60 µmol/L) in 100 µL medium and incubated for 5 days. Cell viability was analyzed by crystal violet staining.

In vitro caspase 3/7 activity

HT1080-FAP, HT1080-WT, or CAF07 cells were seeded (10,000 cells/well) in 100 µL medium in 96-well plates and grown overnight at 37°C. Medium was removed and cells were incubated with 100 µL medium containing either 400 nmol/L of the different antibodies (OMTX005, OMTX705, or idiotype-TAM558), or 60 µmol/L of the free drug (TAM470 or TAM 558) for different exposure times (1, 6, 24, and 48 hours) at 37°C. Caspase 3/7 activity was determined using Caspase-Glo 3/7 Assay according to manufacturer's instructions (Promega). Briefly, 50 µL of medium was removed from each well. Then, 50 µL of Caspase-Glo substrate mix was added to the wells (1:1 ratio) and incubated for 1 hour at room temperature. Luminescence signal, which is proportional to the caspase 3/7 activity level, was measured using Tecan Reader.

In vivo efficacy studies in immunodeficient patient-derived xenograft murine models

Mice were purchased from Envigo and were maintained at the Spanish National Cancer Research Centre (CNIO) animal facility (Association for Assessment and Accreditation of Laboratory Animal Care International accredited) in accordance with the guidelines of the International Guiding Principles for Biomedical Research Involving Animals, developed by the Council for International Organizations of Medical Sciences. All animal experiments were approved by the Competent Authority of Comunidad de Madrid (project PROEX 104/16). Patient-derived xenograft (PDX) models used in this work were established as described previously (25, 26). A summary of the clinical data of the models employed is provided in Supplementary Table S1.

Five-week-old *Foxn1 nu/nu* (nude) female mice were implanted subcutaneously with 2–3 mm^3 tumor pieces of Panc 007, a pancreatic cancer PDX model. When tumors reached a volume of approximately 200 mm^3, mice were randomized into groups (in general $n = 8$/group) and treated with different doses of OMTX705 (10–60 mg/kg) and at different administration regimes (intravenous or intraperitoneal once or twice a week) as single agent or in combination with gemcitabine (50 mg/kg). For the other PDX studies, mice were implanted following the same procedures with the triple-negative breast cancer (TNBC) PDX model (Breast 014), the lung non–small cell lung cancer (NSCLC) PDX model (Lung 024), or the ovarian cancer PDX model (Ovary 020) and randomized to several experimental groups (in general $n = 8$/group). When tumors reached a volume of approximately 200 mm^3, mice were treated with 10 or 30 mg/kg OMTX705 alone or in combination with paclitaxel (7.5 mg/kg). Animals were checked daily for any symptoms of toxicity and body weights were measured twice a week. Tumor volumes were measured with a caliper twice a week using the formula: [(short diameter)^2 × long diameter]/2. Percent tumor growth inhibition (%TGI) values were calculated for each treatment group (T) versus control (C) using initial (i) and final (f) tumor measurements by the equation $\%TGI = 1 - (Tf - Ti)/(Cf - Ci)$.

In vivo efficacy study in mice with humanized immune system

Immunocompromised, 5–8 weeks old female mice (Taconic, NOG) engrafted with unmatched HLA human $CD34^+$ cells, were implanted subcutaneously with 1–1.5 cm^3 tumor fragments of the CTG-0860 NSCLC PDX model (low-passage ImmunoGraft model of human NSCLC obtained from Champions Oncology). When tumors reached approximately 80–200 mm^3, mice were randomized into groups (10 mice/group) for OMTX705 monotherapy, pembrolizumab monotherapy, combination of OMTX705 with pembrolizumab, or control. OMTX705 monotherapy was administered at 20 mg/kg (twice in the first week followed by once weekly for 2 weeks) until day 21. Pembrolizumab was used at the dose of 2.5 mg/kg every 5 days. On day 21, mice treated with OMTX705 monotherapy were randomized to two groups: one group was followed without treatment (OMTX705 3 weeks) and the other group received an additional dose of 10 mg/kg OMTX705 (OMTX705 4 weeks). Similarly, mice with combination treatment were randomized to two groups on day 21: one group was treated with 2.5 mg/kg of pembrolizumab (OMTX705 3 weeks + pembrolizumab) and the other group was treated with 2.5 mg/kg of pembrolizumab and 10 mg/kg OMTX705 for an additional week (OMTX705 4 weeks + pembrolizumab). After the fourth week, groups treated with OMTX705 were maintained in observation without treatment for 20 additional days. Body weights were measured twice a week. Tumor volumes (TV) were measured with a caliper twice a week using the formula: $TV = \text{width}^2 \times \text{length} \times 0.52$. %TGI values were calculated by the formula $\%TGI = 1 - (T_f - T_i)/(C_f - C_i)$.

The numbers of complete responders (CR), partial responders (PR), and tumor-free survivors (TFS) were calculated on day 21. A PR was

Published OnlineFirst March 11, 2020; DOI: 10.1158/1078-0432.CCR-19-2238

defined as a mouse with TV ≤ 30% of TV at day 0 which persisted for two consecutive measurements. CR was defined as a mouse with undetectable TV for two consecutive measurements and TFS were considered mice with a CR that persisted until the study was completed. Additional information on the methods utilized is provided in Supplementary Materials and Materials.

Statistical analysis

Numerical data processing and statistical analysis were performed with GraphPad Prism 7 software; values were expressed as mean ± SE. *P* values were calculated using one-way ANOVA followed by Tukey multiple comparisons test. For flow cytometry and IHC expression data, Mann–Whitney U test and Student *t* test methods were performed, respectively, to determine *P* values.

Results

Generation and characterization of OMTX705 anti-FAP conjugates

We first generated OMTX005, a humanized IgG1 mAb from a mouse anti-FAP antibody (27). A novel cytolysin, TAM470, derived from natural parent tubulysin A and B, was synthesized. TAM470 binds to β-tubulin and destabilizes the α-β heterodimeric form inhibiting tubulin polymerization and microtubule depolymerization, similarly to vinca alkaloids and colchicine (28–31). OMTX005 was further conjugated to TAM470 through Cys-based nondirected conjugation using an optimized protease-cleavable linker vcPABA-$(EG)_3$. The structure of OMTX705 and the main biochemical properties of the ADC are shown in **Fig. 1A** and **B**. A mean drug–antibody ratio (DAR) value of 3.5 was reproducibly obtained between batches, with >95% monomer purity and 5% mean free antibody. Free/unbound drug was below detection level and endotoxin levels were below 1 EU/mL.

The binding and internalization properties of OMTX705 were compared with naked OMTX005 anti-FAP antibody and an isotype/TAM558 control ADC. Antigen recognition and binding were evidenced in ELISA studies with immobilized recombinant FAP (Supplementary Fig. S1A) and in flow cytometry analysis using FAP-expressing cell lines (Supplementary Fig. S1A and S1B). Unconjugated OMTX005 displayed specific binding to both human and murine recombinant FAP proteins in a concentration-dependent manner, with EC_{50} values of 0.33 and 0.25 nmol/L, respectively (Supplementary Fig. S1A), which makes it suitable for preclinical testing in animal models. Furthermore, OMTX705 and OMTX005 bound to HT1080-FAP and to primary CAFs with EC_{50} values of 76 pmol/L and 130 nmol/L, respectively (Supplementary Fig. S1B). This indicates that the conjugation process does not affect the antigen-binding properties of OMTX705. OMTX705 did not bind to HT1080-WT cells. Likewise, the control isotype IgG1 kappa-TAM558 ADC did not show binding. OMTX705 internalized quickly (<6 hours) into primary CAFs, but not the IgG1 kappa-TAM558, suggesting that internalization was FAP dependent. This process was active because rapid internalization was observed at 37°C compared with incubation at 4°C (Supplementary Fig. S1C).

OMTX705 exhibits potent and specific FAP-dependent cytotoxic activity

The activity of OMTX705 was tested *in vitro* in viability assays with primary CAFs, HT1080-FAP, and HT1080-WT cells (**Fig. 1C**). OMTX705 showed a high and FAP-specific cytotoxic activity with an IC_{50} of approximately 230 pmol/L in HT1080-FAP cells and a 500-fold specificity ratio as compared with HT1080-WT cells. No activity was found with the corresponding OMTX005-unconjugated antibody, which did not have any effect in the cell lines tested. Similarly, the isotype IgG1 kappa-TAM558 control ADC induced limited effect at the highest concentration tested (400 nmol/L) in all cell types. Notably, OMTX705 exhibited much lower activity in primary CAFs with IC_{50} value in the range of 400 nmol/L, as compared with the more proliferative HT1080 cells overexpressing FAP. The payload molecules TAM558 and TAM470 were active in all cell types independently of FAP expression demonstrating the lack of specificity of their cytotoxic effect. However, while TAM470 (cytolysin payload without linker) was very effective at all concentrations tested, with no cell viability observed over a concentration range from 1 nmol/L to 60 μmol/L in any cell types, unconjugated TAM558 (TAM470 with linker) showed much lower activity (IC_{50} value of 1–5 μmol/L in all cell types). In addition, caspase 3/7 activity was specifically increased after OMTX705 treatment in HT1080-FAP cells but not in HT1080-WT or CAF07 cells, while TAM470 and TAM558 treatments were able to induce caspase 3/7 activity in all cell types, independently of FAP expression (**Fig. 1D**). Neither isotype IgG1 kappa-TAM558 control ADC nor OMTX005 naked antibody was able to induce caspase activity in any of the cell types tested.

OMTX705 pharmacokinetic characterization indicates high stability in bloodstream

Pharmacokinetic studies were performed to evaluate drug stability in the bloodstream. Mice were treated with a single intravenous injection of either OMTX705 or the corresponding naked antibody OMTX005 at a dose of 25 and 150 μg. Blood samples were collected at different time points and analyzed by a sandwich ELISA using immobilized recombinant FAP protein and horseradish peroxidase (HRP)-labeled anti-human IgG or anti-cytolysin for detection. OMTX705 pharmacokinetic parameters in mice showed a linear, dose-dependent increase in exposure and were similar to unconjugated antibody, with a half-life in mouse serum of 42.6 ± 10.7 hours (**Fig. 1E**). The pharmacokinetic profile of the ADC, detected through recognition of the payload or the Fc region, and the unconjugated antibody are identical, suggesting that there is no release of payload up to 7 days after administration and that OMTX705 is highly stable in the bloodstream.

OMTX705 is efficacious in multiple solid tumor xenografts and exhibits activity in combination with clinically relevant agents

OMTX705 efficacy was studied *in vivo* in PDX models of different tumor types selected for their desmoplastic response, FAP expression level, and resistance to chemo- and immunotherapy (Supplementary Table S1). In a PDX model of pancreatic cancer (Panc 007), single agent administration of OMTX705 at doses ranging from 20 to 60 mg/kg i.v. once weekly for four doses resulted in tumor regressions at doses above 30 mg/kg that lasted at least 5 weeks (**Fig. 2A**). Similar results were observed by intraperitoneal administration with single-agent activity observed at 20 mg/kg (**Fig. 2B**). Furthermore, the combination of OMTX705 (10 mg/kg) with gemcitabine resulted in durable tumor regressions that lasted at least 90 days (**Fig. 2B**). Treatment was well tolerated with no significant weight loss observed (Supplementary Fig. S2A).

Next, we tested cyclic administration of OMTX705 as routinely done in clinical practice. As shown in **Fig. 2C**, OMTX705 treatment was interrupted after 2 weeks (day 16) when tumor growth inhibition was evident. Animals were left untreated for additional 2 weeks and treatment with OMTX705 was resumed on day 29 when tumor regrowth was detectable. Notably, tumor responses were again

Published OnlineFirst March 11, 2020; DOI: 10.1158/1078-0432.CCR-19-2238

observed at day 36 and onwards suggesting lack of resistance to treatment in this model (**Fig. 2C**; Supplementary Fig. S2B).

We further evaluated OMTX705 efficacy in PDX models of other tumor types with desmoplastic reaction, such as NSCLC and TNBC. In the Lung 024 model, single agent OMTX705 (10 mg/kg) resulted in growth inhibition, while paclitaxel monotherapy was less effective. The combination of both agents showed synergistic effects. Single agent OMTX705 at higher dose (30 mg/kg) showed higher efficacy, with no

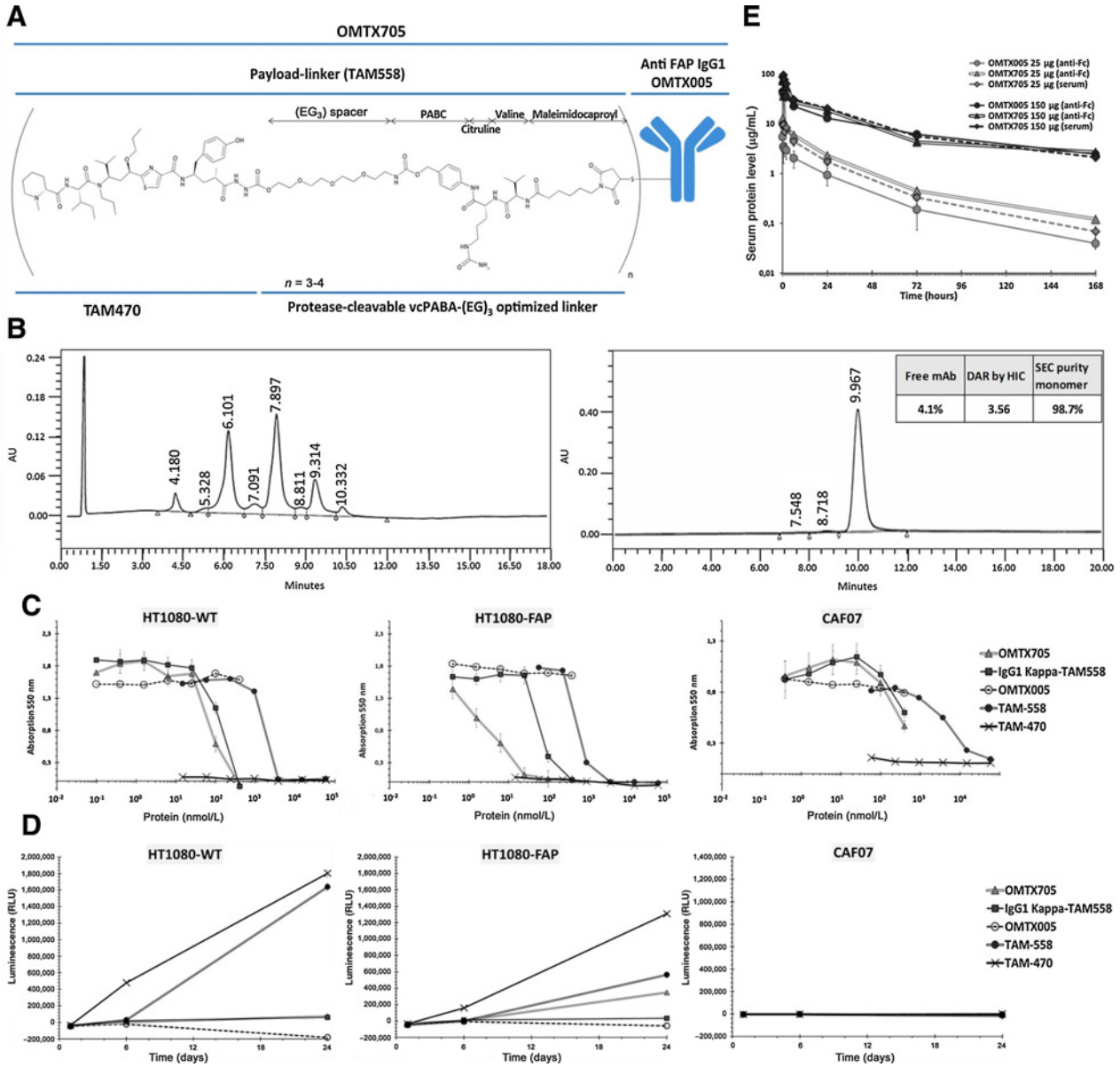

Figure 1.

Generation and characterization of OMTX705. **A,** General structure of OMTX705 ADC. Anti-FAP mAb was linked through CYS-based nondirected conjugation to the synthetic cytolysin, TAM470, using a vcPABA-$(EG)_3$ linker to generate OMTX705 conjugate. **B,** Hydrophobic interaction chromatography (HIC) and size exclusion chromatography (SEC) profiles of OMTX705. Distribution of OMTX705 ADC species and DAR were analyzed through HIC (left). Monomer purity was analyzed through SEC (right). Retention times are indicated for each peak. Percentage of free antibody, mean DAR, and monomer purity values are shown in the table of right panel. **C,** OMTX705 shows a potent and FAP-specific cytotoxic activity. Cell viability in CAF07, HT1080-FAP, and HT1080-WT cells was analyzed via crystal violet staining after exposure to the indicated antibodies or free drug. Cells were treated for 120 hours with a serial dilution of antibodies (starting at 400 nmol/L) or free drugs (starting at 60 µmol/L). Mean ± SD; $n = 3$. **D,** OMTX705 induces caspase 3/7 activity on FAP-expressing cells. Cells were treated with 400 nmol/L of indicated antibody or 60 µmol/L of free drug for different duration. Measured luminescence is proportional to caspase activity level. Mean ± SD; $n = 2$. **E,** Pharmacokinetics of OMTX705. CD-1 mice received a single intravenous injection of OMTX705 or OMTX005 by tail vein as indicated. Blood samples were obtained at different time points up to 7 days, and serum concentrations of the antibodies were determined by sandwich ELISA using either HRP-coupled anti-human Fc (anti-Fc) or rabbit anti-TAM558 cytolysin-p153 polyclonal antibody (serum) in combination with HRP-conjugated anti-rabbit antibody ($n = 3$–6).

Published OnlineFirst March 11, 2020; DOI: 10.1158/1078-0432.CCR-19-2238

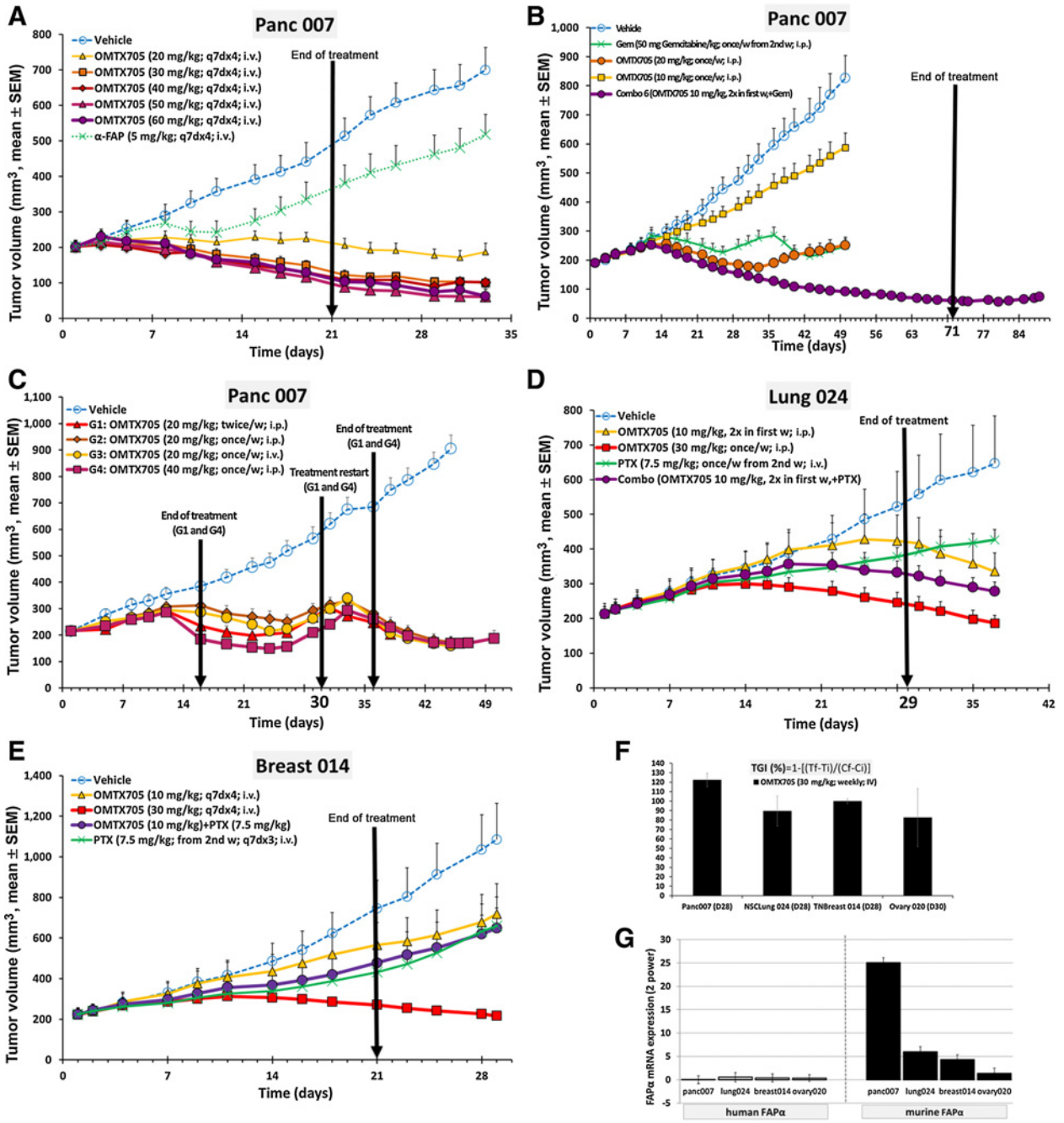

Figure 2.

OMTX705 exhibits potent effect in immunodeficient PDX models of different solid tumors. **A,** Activity of single agent OMTX705 in the PDAC Panc 007 PDX model. OMTX705 was given intravenously (i.v.) once weekly for four doses (q7dx4). Mice in the control groups were treated weekly with vehicle or unconjugated OMTX005 anti-FAP antibody (α-FAP). Treatment started on day 1 and ended on day 21. **B,** Activity of OMTX705 alone or combined with gemcitabine in the Panc 007 PDX model. OMTX705 was administered intraperitoneally (i.p.) once weekly, whereas gemcitabine was administered intraperitoneally weekly starting in the second week. **C,** Cyclic versus continuous OMTX705 treatment. Panc 007 PDX model was treated with OMTX705 at the indicated doses and regimens. OMTX705-treated groups G1 and G4 received treatment for 2 weeks, followed by 2 weeks off treatment, and then 1 week on treatment. Groups G2 and G3 received treatment with OMTX705 at lower dose (20 mg/kg i.v. or i.p.) but without interruption. **D,** Lung adenocarcinoma Lung 024 PDX models treated with OMTX705 alone or combined with paclitaxel (PTX). Paclitaxel alone was ineffective. Combination of paclitaxel with OMTX705 at 10 mg/kg was more effective than either drug alone at the same doses. OMTX705 alone at 30 mg/kg showed higher efficacy. **E,** Breast cancer Breast 014 PDX models treated with OMTX705 alone or combined with paclitaxel. OMTX705 at 30 mg/kg demonstrated the highest tumor regression rate in this model, whereas paclitaxel with or without a lower dose of OMTX705 was less effective. **F,** TGI in different PDX models. TGI was calculated using TV measured 1 week after last dose of OMTX705. **G,** FAP mRNA expression in tumors from all PDX models tested. Expression of murine versus human FAP was detected by qRT-PCR using specific primers. FAP levels are expressed with respect to GAPDH levels present in each sample. Only murine FAP expression was found in the tumor stroma of those models.

Published OnlineFirst March 11, 2020; DOI: 10.1158/1078-0432.CCR-19-2238

apparent toxicity (**Fig. 2D**; Supplementary Fig. S2C). Similarly, in the TNBC PDX model Breast 014 we observed that single agent OMTX705 at a dose of 30 mg/kg had the best efficacy, while a lower dose (10 mg/kg) with or without paclitaxel had more limited effects (**Fig. 2E**; Supplementary Fig. S2D). TGI values of single agent OMTX705 in those models are shown in **Fig. 2**F. While the agent was highly effective across all models with TGI above 80%, including the PDX model for ovarian cancer Ovary 020, Panc 007 was the most sensitive (**Fig. 2F**; Supplementary Fig. S3). Intriguingly, this was the model with the highest mRNA murine FAP expression (**Fig 2G**).

OMTX705 promotes immunomodulation of tumor microenvironment and increases the effect of pembrolizumab in immunocompetent models

To determine the potential involvement of the immune system in the antitumoral effects of OMTX705, we implanted the FAP-positive human NSCLC PDX model (CTG-0860) into mice in which the immune system had been reconstituted by engraftment with human CD34$^+$ hematopoietic stem cells (low-passage ImmunoGraft model, Champions Oncology). Tumor-bearing mice were treated with either OMTX705 as single agent or in combination with pembrolizumab. Single agent pembrolizumab was ineffective in this model (**Fig. 3A–C**). However, OMTX705 at a dose of 20 mg/kg (for 3 or 4 weeks) with or without pembrolizumab caused substantial tumor regressions by day 21 as compared with control or pembrolizumab alone (**Fig. 3A**). While single agent OMTX705 and OMTX705 with pembrolizumab combination had similar TGI on day 21, monotherapy only caused partial responses while the combination resulted in a complete response CR in 1 of the 5 mice treated (**Fig. 3B**). Notably, OMTX705 showed an overall higher antitumor activity in mice bearing humanized immune system, with tumor regressions seen in all animals with the dose of 20 mg/kg weekly, whereas in the immunodeficient models the same dose resulted in a stable disease phenotype (**Fig. 2A–E**).

After treatment discontinuation on day 25, mice treated with OMTX705 alone displayed a slow but steady tumor regrowth by day 45, while animals treated with OMTX705 + pembrolizumab combination maintained durable responses for more than 3 weeks past the last treatment. Overall, an increase in tumor regression rate was observed with OMTX705 + pembrolizumab with 90% of mice in the combination group achieving a >75% reduction in tumor burden as compared with 65% of the animals in the OMTX705 monotherapy group. Furthermore, 20% of mice in the combination group achieved

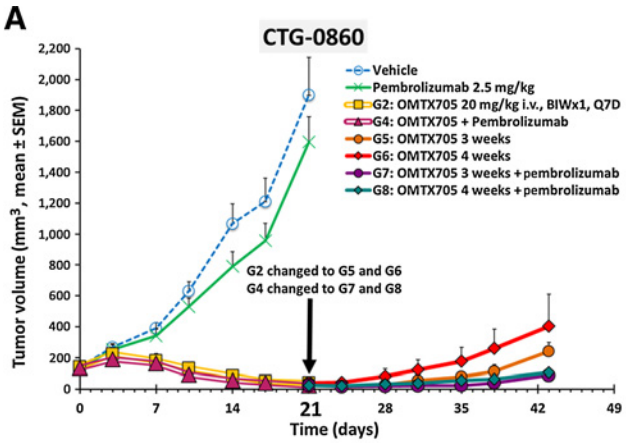

B

Treatment	n at day 21	Dose (mg/kg)	Dosing Schedule	Tumor volume (day 21) Mean±SEM (mm^3)	P_{adj}*	%TGI	Days 0-21 # PR/CR/TFS
Vehicle 1 Vehicle 2	10	0 0	i.v., 4 doses i.p., 4 doses	1,899 ± 244	-	-	0 / 0 / 0
OMTX705	9	20	i.v., 4 doses	40 ± 16	< 0.0001	106	5 / 0 / 0
Pembro.	9	2.5	i.p., 4 doses	1,597 ± 170	0.5054	16	0 / 0 / 0
OMTX705 pembro.	10	20 2.5	i.v., 4 doses i.p., 4 doses	24 ± 7	< 0.0001	106	4 / 1 / 0

* One-way ANOVA followed by Tukey multiple comparisons test.

C

Treatment	% of mice according to % tumor regression >25%	>50%	>75%	100% (complete response)
Vehicle	0%	0%	0%	0%
Pembrolizumab	0%	0%	0%	0%
OMTX705 3-4 weeks	11%	22%	56%	11%
OMTX705 3-4 weeks + pembro.	0%	10%	70%	20%

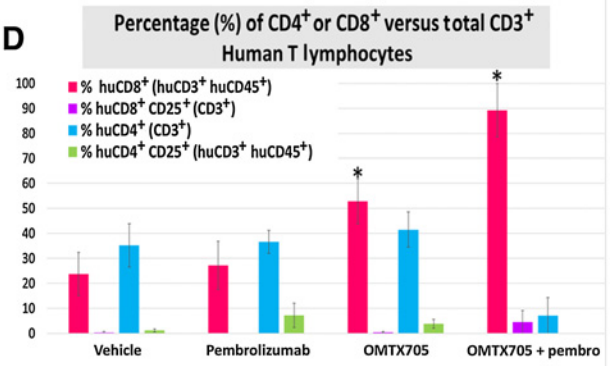

Figure 3.

Antitumoral effect of OMTX705 in a humanized PDX lung cancer model. **A,** Mice bearing NSCLC CTG-0860 PDX tumors were treated with vehicle, OMTX705 monotherapy, pembrolizumab (pembro) monotherapy, or OMTX705/pembrolizumab combination (n = 10/group). On day 21, mice treated with OMTX705 monotherapy (G2) were randomized to two groups: one group was followed without treatment (G5, OMTX705 3 weeks) and the other group received an additional dose of OMTX705 (G6, OMTX705 4 weeks). Similarly, mice with combination treatment (G4) were randomized to two groups on day 21: one group was treated with additional dose of pembrolizumab (G7, OMTX705 3 weeks + pembrolizumab) and the other group was treated with pembrolizumab and OMTX705 for an additional week (G8, OMTX705 4 weeks + pembrolizumab). **B,** Summary of antitumor activity on day 21. *, one-way ANOVA followed by Tukey multiple comparisons test with %TGI and number of animals with partial response, complete response, or tumor free in each group is shown. **C,** Percentage of mice with each category of tumor regression in the different treatment groups. **D,** Percentage of different subtypes of CD3$^+$ T cells in CTG-0860 PDX tumors from different groups of treatment analyzed through FACS. Mann–Whitney U test analysis of huCD8$^+$ (huCD3$^+$ huCD45$^+$ markers) shows a significant increase in OMTX705 (P = 0.05) and OMTX705 + pembrolizumab (P = 0.015) dosed groups as compared with vehicle. i.v., intravenous; i.p., intraperitoneal.

Published OnlineFirst March 11, 2020; DOI: 10.1158/1078-0432.CCR-19-2238

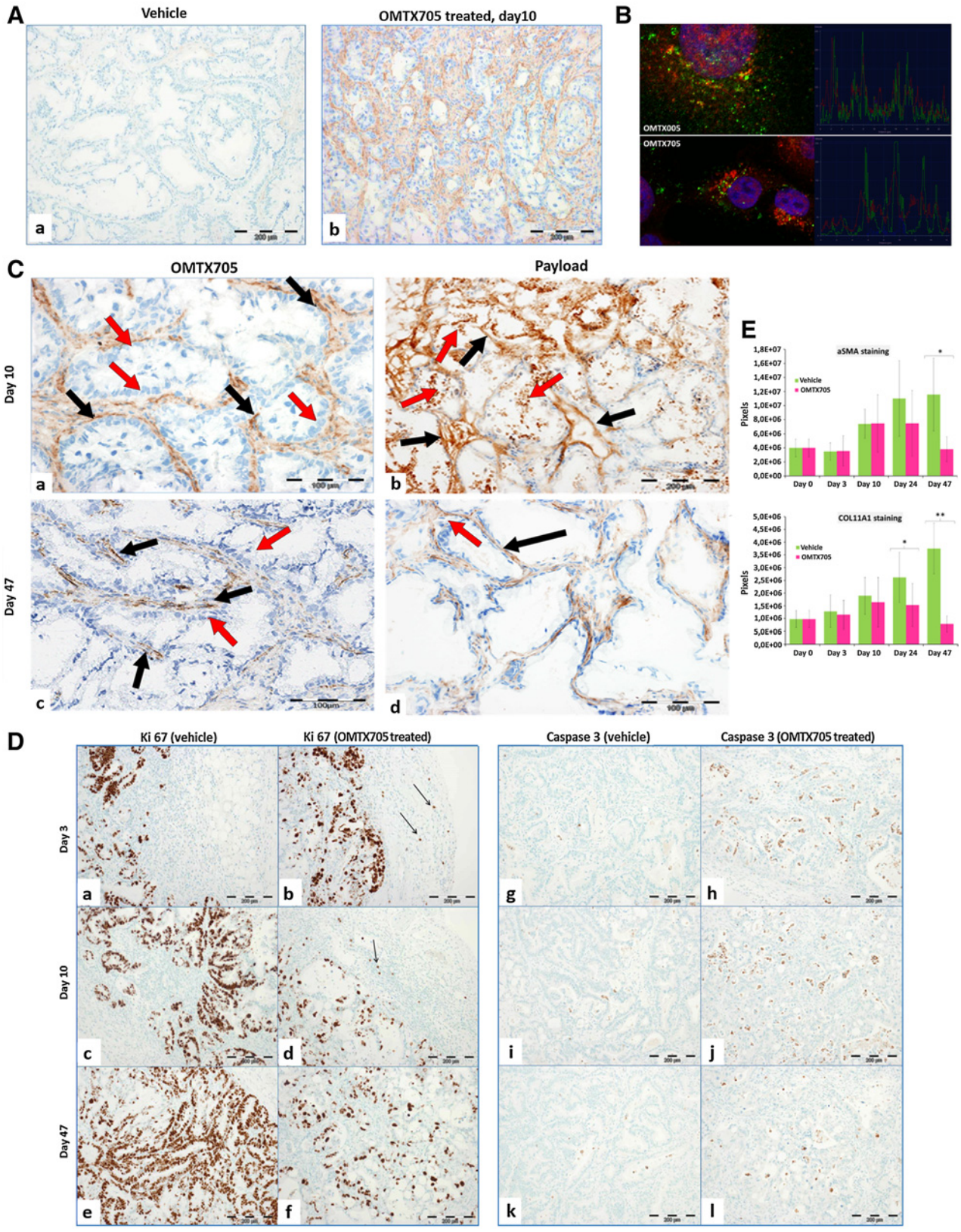

Published OnlineFirst March 11, 2020; DOI: 10.1158/1078-0432.CCR-19-2238

complete response versus 10% in OMTX705 group (**Fig. 3C**). Importantly, FAP expression by IHC with OMTX005 anti-FAP antibody showed expression predominantly in the intratumoral fusiform stromal cells rather than malignant epithelial tumor cells in those humanized models (Supplementary Fig. S4), suggesting that the antitumoral response observed with OMTX705 is likely driven through FAP-expressing stromal fibroblasts.

We observed a significant increase in $CD8^+$ cytotoxic T-cell infiltration within tumors treated with OMTX705 as single agent ($P = 0.05$), which was further enhanced in the OMTX705 + pembrolizumab combination group ($P = 0.015$; **Fig. 3D**). We also observed a nonstatistical increase in the infiltration of $CD8^+CD25^+$ cytotoxic memory T cells in the mice treated with OMTX705 + pembrolizumab, which experienced a delay in tumor recurrence after treatment discontinuation. The proportion of $CD4^+$ Th cells and $CD4^+CD25^+$ regulatory T (Treg) cell infiltration did not show any significant change upon OMTX705 treatment as single agent, while it was reduced in the OMTX705 + pembrolizumab group. These results suggest that some of the antitumor effect observed with OMTX705 + pembrolizumab in this model may derive from a modulation of the tumor milieu that is primarily dominated by recruitment of $CD8^+$ cytotoxic with lesser contribution from $CD4^+$ cells.

Mechanism of OMTX705 antitumoral efficacy

To understand the mechanisms of action of OMTX705, we performed *in vivo* studies to support the FAP binding results obtained *in vitro* (Supplementary Fig. S1). Mice bearing the Panc 007 model were treated with weekly intravenous OMTX705 at 30 mg/kg and tumors were collected at day 3, 10, 24, or 47 after treatment commencement. Tumors were excised and formalin-fixed, paraffin-embedded sections were stained with an anti-human IgG antibody to detect FAP-bound OMTX705. As shown in **Fig. 4A**, OMXTX705 bound predominantly to the fusiform intratumoral stromal cells, with no staining observed in the malignant epithelial cells. Double labeling immunofluorescence studies in HT1080-FAP cells showed that OMTX705 is internalized upon binding and localizes in the late endosome where TAM470, the active payload, is released through its protease-cleavable linker (**Fig. 4B**; Supplementary Fig. S5).

To further elucidate its mechanism of action *in vivo*, Panc 007 tumors were collected at different time points after treatment with OMTX705. IHC staining shows TAM558 payload in OMTX705-treated tumor samples but not in vehicle-treated tumors, as expected (**Fig. 4C**; Supplementary Fig. S6). In addition, a highly specific staining of payload was observed in fusiform stromal cells from day 3, and in tumor cells from day 10 (Supplementary Fig. S6). Furthermore, we observed a significant decrease in Ki-67^+ tumor cells at day 24 and substantial morphologic alterations which are consistent with tumor cell growth inhibition (**Fig. 4D**). This decrease in tumor cell proliferation upon OMTX705 treatment also correlated with an increase in caspase-3 staining from day 3 up to day 24. Active caspase-3–positive staining was found only in malignant epithelial cells from OMTX705-treated samples. No staining appeared to be detected in vehicle-treated tumors and in stromal fibroblasts (**Fig. 4D**). Moreover, we observed tumor stroma depletion as evidenced by the decrease expression of the specific activated CAF markers αSMA and COL11A1 (**Fig. 4E**). This stroma reduction was detectable at day 24, with significantly highest depletion at day 47 (3 weeks after end of treatment; $P = 0.003$), and similarly correlated to tumor growth inhibition and long-lasting effect after end of treatment (**Fig. 4E**).

Discussion

Targeting desmoplastic stroma is a compelling therapeutic strategy in oncology because of its critical role in tumor progression and drug resistance. Nonetheless, recent attempts to target stromal elements have given contradicting results and, in certain occasions, promoted worse outcomes. For instance, attempts to target αSMA-expressing CAFs promoted increased tumor invasiveness leading to decreased survival in tumor-bearing mice (19). Other groups have shown that deletion of *sonic Hedgehog* predictably suppressed stromal desmoplasia, but paradoxically promoted the growth of more aggressive and undifferentiated tumors, underscoring the need for caution when targeting CAFs and the stromal compartment more broadly (32, 33).

FAP has a restricted expression in stromal CAFs and plays a pivotal role in tumorigenesis and drug resistance (7). We exploited these unique features to devise a novel ADC-targeting FAP in tumor stroma fibroblasts. Previous approaches blocking FAP have failed in phase II clinical trials due to lack of efficacy (22–24). Here, the strategy was not aimed at blocking FAP, but at using FAP as a docking for a CAFspecific internalization of a potent cytotoxic payload. OMTX705 is a novel ADC formed by a new anti-FAP humanized mAb that has been conjugated to the cytolysin TAM470, a novel microtubule inhibitor that induces cell-cycle arrest in G_2–M-phase, ultimately triggering apoptosis (29).

Treatment with OMTX705 showed remarkable therapeutic benefit, with rapid onset of action and long-lasting suppression of tumor growth in PDXs of pancreas, lung, breast, and ovary cancers as a single agent and with evidence of synergist effect when combined with clinically relevant chemotherapeutic drugs. Robust TGI was observed with once and twice weekly dosing

Figure 4.

Mechanism of action of OMTX705. **A,** Localization of OMTX705 in treated PDX tumors. Detection of OMTX705 binding *in vivo* at 48 hours after intravenous administration using IHC staining on FFPE sections of tumor samples excised at day 10 of treatment from either vehicle- (a) or OMTX705-treated Panc 007 PDX models (b), with HRP-coupled anti-hu IgG secondary antibody. Magnification, 10×. **B,** Immunofluorescence staining of OMTX005 or OMTX705 in HT1080-FAP cells analyzed by confocal microscopy. OMTX005 and OMTX705 were detected with FITC-labeled anti-human Fab antibody (green). As late endosome marker, rabbit anti-Rab7 antibody in combination with a PE-labeled anti-rabbit antibody (red), was used. Nuclei were stained with DAPI (blue). Chromatogram shows distribution of different fluorophore intensities of a confocal layer across the cell (red line). **C,** Analysis of payload versus OMTX705 distribution through IHC staining of vehicle- versus OMTX705-treated tumor samples from Panc 007 PDX mice extracted at day 10 and 47 of treatment. OMTX705-treated tumor stained with anti-huIgG (OMTX705) and anti-TAM558 p153 (payload) reveals the location of both OMTX705 ADC and payload. Black arrows, stromal fibroblasts; red arrows, malignant epithelial cells. **D,** IHC staining in tumor samples from Panc 007 PDX mice extracted after vehicle or OMTX705 treatment. Ki67 (left). Active caspase 3 (right). Black arrows, positive activated fibroblasts and/or immune cells. **E,** Graphs show level of αSMA and COL11A1 expression detected by IHC in FFPE sections of Panc 007 PDX tumors excised at different days following vehicle or OMTX705 treatment. Graphs represent the number of pixels on total positive surface, including weak up to strong positivity ($n = 10$). Significant decrease in αSMA (70%) and COL11A1 (80%) expression is observed at day 47 in OMTX705-treated versus vehicle-treated animals ($P = 0.003$; Student t test).

schedules. These findings have important implications for the clinical development of OMTX705 as they offer the possibility of greater flexibility in dosing schedules to mitigate any potential on-target toxicities without sacrificing efficacy. Treatment was well tolerated considering the cross-reactivity with endogenous murine FAP. Notably, even after periods of treatment discontinuation, OMTX705 maintained efficacy upon reintroduction with no evidence of drug resistance, providing clear rationale for clinical testing using discontinuous dosing strategies.

The absence of resistance in our models can be explained, at least in part, by the targeting of the stroma which is a relatively genetically stable compartment as compared with malignant cells (34), as well as the use of a cytolysin as the effector molecule. These synthetic analogues of the natural tubulysin are not substrate of the multidrug resistance efflux transporters P-glycoprotein, therefore providing a treatment that does not generate resistance upon tumor recurrence (29). Intriguingly, we observed that the rate of growth inhibition was the highest in the pancreatic cancer models which correlates with the high FAP mRNA expression in this model. These data support future studies to investigate the potential role of FAP expression as a biomarker of response to OMTX705.

Mechanistically, the staining pattern obtained suggests that OMTX705 specifically targets fusiform FAP^+ stromal cells surrounding malignant epithelial cells, with no binding to the latter. However, because we have not performed dual staining experiments yet, this contention remains speculative at this time. OMTX705 is rapidly internalized in FAP (+) fibroblasts to late endosomes where the active effector molecule is released. Importantly, while the staining of OMTX705 was predominant in stromal cells, those do not appear to be killed by OMTX705, perhaps because the majority are non- or low-proliferating cells. Conversely, malignant epithelial cells in the vicinity, which have higher proliferating rate as evidenced by positive Ki-67, are killed through apoptosis upon OMTX705 treatment. These findings may suggest a bystander effect with FAP^+ tumor stroma fibroblasts acting as a reservoir of the cytotoxic payload which, due to its lipophilic properties, may be released locally promoting the killing of the nearby rapidly proliferating malignant epithelial cells. A more delayed stroma depletion, as evidenced by the decreased expression of the CAF markers αSMA and COL11A1, was also observed 3 weeks after treatment interruption, correlating with tumor growth inhibition and long-lasting effect after end of treatment. In addition to this proposed mechanism of action in which OMTX705 binding to stromal cells leads to local release of the drug within the tumor, killing nearby malignant epithelial cells, an alternative explanation involves the disruption of paracrine signaling of stromal cells, impairing epithelial cell biology. Future studies will be necessary to dissect which mechanism is chiefly involved in pancreatic cancer.

FAP-expressing stromal cells are also involved in the modulation of the antitumor immune response, adding yet another aspect to the multiple contributions of FAP to cancer progression. Here, we showed that OMTX705 enhanced the effect of anti-PD-1 therapy in immunocompetent models with a robust increase in $CD8^+$ cytotoxic T-cell tumor infiltration noted following OMTX705 monotherapy or combined with pembrolizumab. We also noted a non-significant increase in $CD8^+CD25^+$ memory T cells following OMTX705/pembrolizumab combination that may contribute to the delay in tumor progression observed after treatment discontinuation. These results are consistent with previous reports showing that FAP^+ CAFs suppress antitumor immunity through modulation of TNFα and IFNγ, which are involved in $CD8^+$ T-cell–dependent killing of cancer cells (7, 35). Similarly, targeting of CAF secretome using a CXCR4 inhibitor to block CXCL12 from FAP^+ cells has been shown to synergize with anti-PD-L1 therapy in a transgenic mouse model of lung cancer (18). We also showed that $CD4^+$ Th cells and $CD4^+$ $CD25^+$ Treg infiltration did not show any significant changes upon OMTX705 treatment as single agent, while it was reduced in the OMTX705 + pembrolizumab groups. These results are consistent with previous reports showing that genetic ablation of FAP^+ cells did not alter the proportions of $CD4^+$ T cells or $CD4^+$ $Foxp3^+$ Tregs (7), suggesting that tumor cell death induced by anti-FAP therapy does not involve a rapid increase of effector $CD4^+$ T cells or decrease of suppressive T cells.

Of further relevance, highly potent microtubule-depolymerizing compounds such as TAM470 cytolysin payload have been shown to activate dendritic cell maturation through the induction of tumor antigen–specific T cells, adding to their direct cytotoxic antitumor effect (36). Specifically, ADCs using tubulysin payloads displayed higher antitumoral activity when used in immunocompetent versus immunodeficient mice and were found to induce a potent immunomodulation of lymphoid and myeloid cells (37). These observations may help to explain the increased efficacy of OMTX705 in our model with humanized immune system, with its associated induction of $CD8^+$ T-cell infiltration and the long-lasting antitumoral effect presented here. While our *in vivo* studies using mice with humanized immune system offered insights on the potential involvement of the immune system in the antitumoral effects of OMTX705, future studies with fully immunocompetent models will be necessary to thoroughly describe the effects of this ADC in the immune tumor microenvironment.

In conclusion, OMTX705 is a novel humanized anti-FAP antibody conjugated to the cytolysin TAM470, which induces marked tumor regressions in PDX models of pancreatic, lung, breast, and ovarian cancers. In an immunocompetent model resistant to PD-1 inhibition, OMTX705 induced complete regression and significantly delayed tumor progression through likely a $CD8^+$ T-cell–dependent immunomodulation. Overall, these data indicate that FAP targeting with OMTX705 represents a novel and potent strategy for cancer treatment including solid tumors resistant to chemo- or immunotherapy.

Disclosure of Potential Conflicts of Interest

M. Fabre is an employee/paid consultant for Oncomatryx Biopharma S.L. C. Ferrer is an employee/paid consultant for Oncomatryx. S. Domínguez-Hormaetxe and L. Murias are employees/paid consultants for Oncomatryx Biopharma S.L. R.E. Kontermann is an employee/paid consultant for and reports receiving commercial research grants from Oncomatryx. K. Pfizenmaier reports receiving commercial research grants from and holds ownership interest (including patents) in Oncomatryx. L. Simon is an employee/paid consultant for and holds ownership interest (including patents) in Oncomatryx Biopharma S.L., Patia Biopharma, Sa de CV, Patia Europe SL, SunRock Biopharma SL, Helenes Ventures SL, Nelum Inc., and Permedika entrepeneurs SL. M. Hidalgo is an employee/paid consultant for Takeda, Agenus, InxMed, Pharmacy, Oncomatryx Biopharma S.L., and BioOncotech; reports receiving commercial research grants from Bioline; and holds ownership interest (including patents) in Agenus, Nelum, Pharmacy, Champions Oncology, and Myriad. No potential conflicts of interest were disclosed by the other authors.

Authors' Contributions

Conception and design: M. Fabre, C. Ferrer, S. Domínguez-Hormaetxe, R.E. Kontermann, M.dM. Vivanco, L. Simon, M. Hidalgo

Development of methodology: C. Ferrer, O. Seifert, S.Y. Lee, M.dM. Vivanco, M. Abbas, M. Hidalgo

Acquisition of data (provided animals, acquired and managed patients, provided facilities, etc.): L. Murias, S.A. Eisler, S.Y. Lee, M.dM. Vivanco, P.P. López-Casas, M. Hidalgo
Analysis and interpretation of data (e.g., statistical analysis, biostatistics, computational analysis): M. Fabre, C. Ferrer, S. Domínguez-Hormaetxe, O. Seifert, R.E. Kontermann, S.Y. Lee, M.dM. Vivanco, M. Hidalgo
Writing, review, and/or revision of the manuscript: M. Fabre, C. Ferrer, S. Domínguez-Hormaetxe, B. Bockorny, O. Seifert, R.E. Kontermann, K. Pfizenmaier, M.dM. Vivanco, P.P. López-Casas, S. Perea, W. Richter, L. Simon, M. Hidalgo
Administrative, technical, or material support (i.e., reporting or organizing data, constructing databases): M. Fabre, C. Ferrer, S. Domínguez-Hormaetxe, O. Seifert, K. Pfizenmaier, M. Hidalgo
Study supervision: M. Fabre, C. Ferrer, L. Simon, M. Hidalgo

Acknowledgments

This work was supported by grants from the Government of the Autonomous Community of the Basque Country; the Department of Industry, Tourism and Trade (Etortek); and SAF2017-84934-R (to M. dM. Vivanco), as well as from HAZITEK program to Oncomatryx.

The costs of publication of this article were defrayed in part by the payment of page charges. This article must therefore be hereby marked *advertisement* in accordance with 18 U.S.C. Section 1734 solely to indicate this fact.

Received July 12, 2019; revised December 2, 2019; accepted March 6, 2020; published first March 11, 2020.

References

1. Pietras K, Ostman A. Hallmarks of cancer: interactions with the tumor stroma. Exp Cell Res 2010;316:1324–31.
2. Kalluri R, Zeisberg M. Fibroblasts in cancer. Nat Rev Cancer 2006;6:392–401.
3. Orimo A, Gupta PB, Sgroi DC, Arenzana-Seisdedos F, Delaunay T, Naeem R, et al. Stromal fibroblasts present in invasive human breast carcinomas promote tumor growth and angiogenesis through elevated SDF-1/CXCL12 secretion. Cell 2005;121:335–48.
4. Joyce JA, Pollard JW. Microenvironmental regulation of metastasis. Nat Rev Cancer 2009;9:239–52.
5. Strell C, Rundqvist H, Ostman A. Fibroblasts–a key host cell type in tumor initiation, progression, and metastasis. Ups J Med Sci 2012;117:187–95.
6. Horimoto Y, Polanska UM, Takahashi Y, Orimo A. Emerging roles of the tumor-associated stroma in promoting tumor metastasis. Cell Adh Migr 2012;6:193–202.
7. Kraman M, Bambrough PJ, Arnold JN, Roberts EW, Magiera L, Jones JO, et al. Suppression of antitumor immunity by stromal cells expressing fibroblast activation protein-alpha. Science 2010;330:827–30.
8. Meads MB, Gatenby RA, Dalton WS. Environment-mediated drug resistance: a major contributor to minimal residual disease. Nat Rev Cancer 2009;9:665–74.
9. Olive KP, Jacobetz MA, Davidson CJ, Gopinathan A, McIntyre D, Honess D, et al. Inhibition of Hedgehog signaling enhances delivery of chemotherapy in a mouse model of pancreatic cancer. Science 2009;324:1457–61.
10. Acharyya S, Oskarsson T, Vanharanta S, Malladi S, Kim J, Morris PG, et al. A CXCL1 paracrine network links cancer chemoresistance and metastasis. Cell 2012;150:165–78.
11. Crawford Y, Kasman I, Yu L, Zhong C, Wu X, Modrusan Z, et al. PDGF-C mediates the angiogenic and tumorigenic properties of fibroblasts associated with tumors refractory to anti-VEGF treatment. Cancer Cell 2009;15:21–34.
12. Straussman R, Morikawa T, Shee K, Barzily-Rokni M, Qian ZR, Du J, et al. Tumour micro-environment elicits innate resistance to RAF inhibitors through HGF secretion. Nature 2012;487:500–4.
13. Kim EJ, Sahai V, Abel EV, Griffith KA, Greenson JK, Takebe N, et al. Pilot clinical trial of hedgehog pathway inhibitor GDC-0449 (vismodegib) in combination with gemcitabine in patients with metastatic pancreatic adenocarcinoma. Clin Cancer Res 2014;20:5937–45.
14. Hingorani SR, Zheng L, Bullock AJ, Seery TE, Harris WP, Sigal DS, et al. HALO 202: randomized phase II study of PEGPH20 plus Nab-paclitaxel/gemcitabine versus Nab-paclitaxel/gemcitabine in patients with untreated, metastatic pancreatic ductal adenocarcinoma. J Clin Oncol 2018;36:359–66.
15. Sherman MH, Yu RT, Engle DD, Ding N, Atkins AR, Tiriac H, et al. Vitamin D receptor-mediated stromal reprogramming suppresses pancreatitis and enhances pancreatic cancer therapy. Cell 2014;159:80–93.
16. Gunderson AJ, Kaneda MM, Tsujikawa T, Nguyen AV, Affara NI, Ruffell B, et al. Bruton tyrosine kinase-dependent immune cell cross-talk drives pancreas cancer. Cancer Discov 2016;6:270–85.
17. Jiang H, Hegde S, Knolhoff BL, Zhu Y, Herndon JM, Meyer MA, et al. Targeting focal adhesion kinase renders pancreatic cancers responsive to checkpoint immunotherapy. Nat Med 2016;22:851–60.
18. Feig C, Jones JO, Kraman M, Wells RJ, Deonarine A, Chan DS, et al. Targeting CXCL12 from FAP-expressing carcinoma-associated fibroblasts synergizes with anti-PD-L1 immunotherapy in pancreatic cancer. Proc Natl Acad Sci U S A 2013;110:20212–7.
19. Ozdemir BC, Pentcheva-Hoang T, Carstens JL, Zheng X, Wu CC, Simpson TR, et al. Depletion of carcinoma-associated fibroblasts and fibrosis induces immunosuppression and accelerates pancreas cancer with reduced survival. Cancer Cell 2014;25:719–34.
20. Niedermeyer J, Scanlan MJ, Garin-Chesa P, Daiber C, Fiebig HH, Old LJ, et al. Mouse fibroblast activation protein: molecular cloning, alternative splicing and expression in the reactive stroma of epithelial cancers. Int J Cancer 1997;71:383–9.
21. Brennen WN, Isaacs JT, Denmeade SR. Rationale behind targeting fibroblast activation protein-expressing carcinoma-associated fibroblasts as a novel chemotherapeutic strategy. Mol Cancer Ther 2012;11:257–66.
22. Scott AM, Wiseman G, Welt S, Adjei A, Lee FT, Hopkins W, et al. A phase I dose-escalation study of sibrotuzumab in patients with advanced or metastatic fibroblast activation protein-positive cancer. Clin Cancer Res 2003;9:1639–47.
23. Adams S, Miller GT, Jesson MI, Watanabe T, Jones B, Wallner BP. PT-100, a small molecule dipeptidyl peptidase inhibitor, has potent antitumor effects and augments antibody-mediated cytotoxicity via a novel immune mechanism. Cancer Res 2004;64:5471–80.
24. Ostermann E, Garin-Chesa P, Heider KH, Kalat M, Lamche H, Puri C, et al. Effective immunoconjugate therapy in cancer models targeting a serine protease of tumor fibroblasts. Clin Cancer Res 2008;14:4584–92.
25. Rubio-Viqueira B, Jimeno A, Cusatis G, Zhang X, Iacobuzio-Donahue C, Karikari C, et al. An *in vivo* platform for translational drug development in pancreatic cancer. Clin Cancer Res 2006;12:4652–61.
26. Hidalgo M, Bruckheimer E, Rajeshkumar NV, Garrido-Laguna I, De Oliveira E, Rubio-Viqueira B, et al. A pilot clinical study of treatment guided by personalized tumorgrafts in patients with advanced cancer. Mol Cancer Ther 2011;10:1311–6.
27. Brocks B, Garin-Chesa P, Behrle E, Park JE, Rettig WJ, Pfizenmaier K, et al. Species-crossreactive scFv against the tumor stroma marker "fibroblast activation protein" selected by phage display from an immunized FAP-/- knock-out mouse. Mol Med 2001;7:461–9.
28. Sasse F, Steinmetz H, Heil J, Hofle G, Reichenbach H. Tubulysins, new cytostatic peptides from myxobacteria acting on microtubuli. Production, isolation, physico-chemical and biological properties. J Antibiot 2000;53:879–85.
29. Khalil MW, Sasse F, Lunsdorf H, Elnakady YA, Reichenbach H. Mechanism of action of tubulysin, an antimitotic peptide from myxobacteria. Chembiochem 2006;7:678–83.
30. Kaur G, Hollingshead M, Holbeck S, Schauer-Vukasinovic V, Camalier RF, Domling A, et al. Biological evaluation of tubulysin A: a potential anticancer and antiangiogenic natural product. Biochem J 2006;396:235–42.
31. Kubicek K, Grimm SK, Orts J, Sasse F, Carlomagno T. The tubulin-bound structure of the antimitotic drug tubulysin. Angew Chem Int Ed Engl 2010;49:4809–12.
32. Rhim AD, Oberstein PE, Thomas DH, Mirek ET, Palermo CF, Sastra SA, et al. Stromal elements act to restrain, rather than support, pancreatic ductal adenocarcinoma. Cancer Cell 2014;25:735–47.

33. Lee JJ, Perera RM, Wang H, Wu DC, Liu XS, Han S, et al. Stromal response to Hedgehog signaling restrains pancreatic cancer progression. Proc Natl Acad Sci U S A 2014;111:E3091–100.
34. Du H, Che G. Genetic alterations and epigenetic alterations of cancer-associated fibroblasts. Oncol Lett 2017;13:3–12.
35. Zhang B, Karrison T, Rowley DA, Schreiber H. IFN-gamma- and TNF-dependent bystander eradication of antigen-loss variants in established mouse cancers. J Clin Invest 2008;118:1398–404.
36. Muller P, Martin K, Theurich S, Schreiner J, Savic S, Terszowski G, et al. Microtubule-depolymerizing agents used in antibody-drug conjugates induce antitumor immunity by stimulation of dendritic cells. Cancer Immunol Res 2014;2:741–55.
37. Rios-Doria J, Harper J, Rothstein R, Wetzel L, Chesebrough J, Marrero A, et al. Antibody-drug conjugates bearing pyrrolobenzodiazepine or tubulysin payloads are immunomodulatory and synergize with multiple immunotherapies. Cancer Res 2017;77:2686–98.

AACR American Association for Cancer Research

Clinical Cancer Research

OMTX705, a Novel FAP-Targeting ADC Demonstrates Activity in Chemotherapy and Pembrolizumab-Resistant Solid Tumor Models

Myriam Fabre, Cristina Ferrer, Saioa Domínguez-Hormaetxe, et al.

Clin Cancer Res Published OnlineFirst March 11, 2020.